Volume 53 | Number 28 | 11 April 2017 | Pages 3905–4044

ChemComm

Chemical Communications

rsc.li/chemcomm

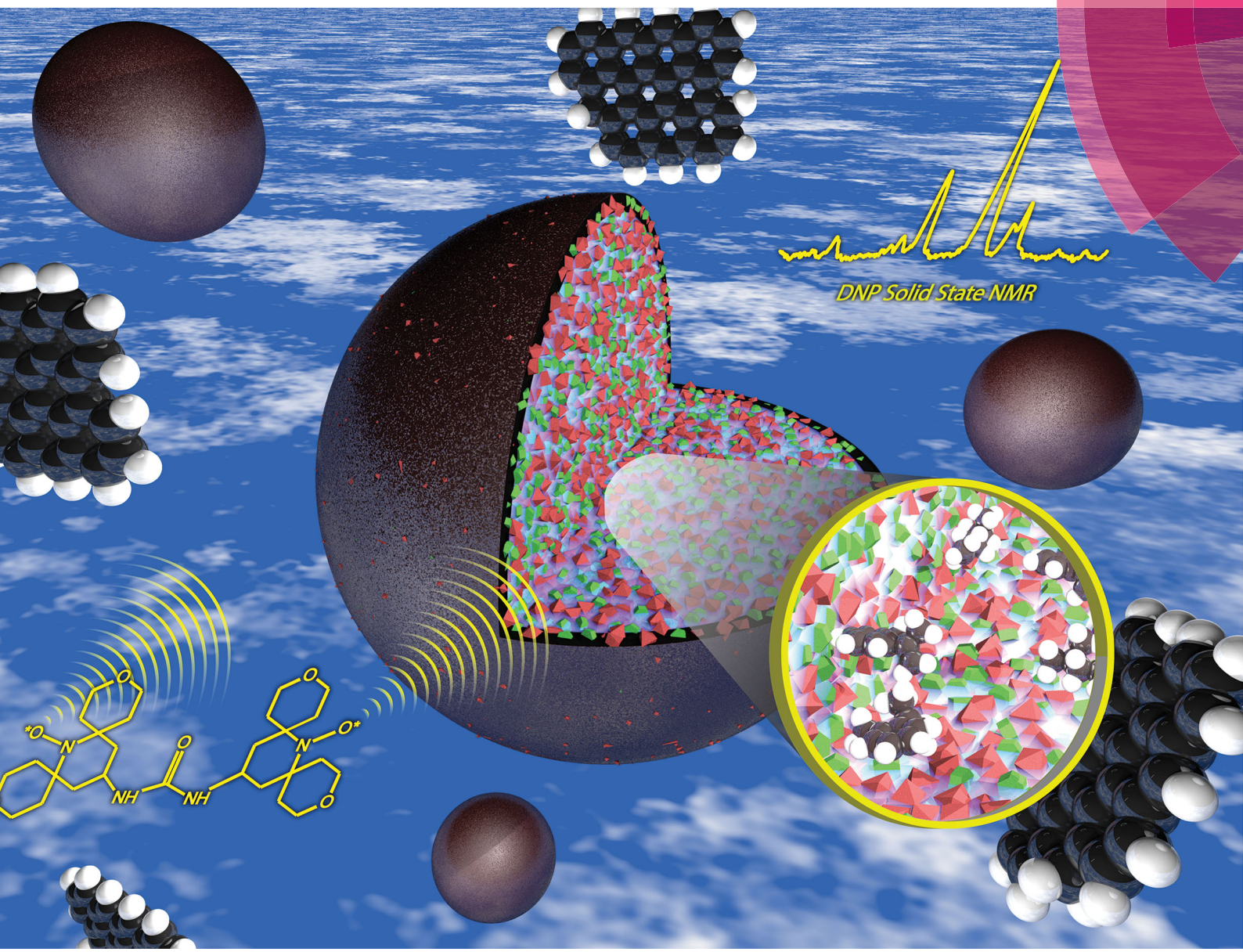

ISSN 1359-7345

ROYAL SOCIETY OF CHEMISTRY

COMMUNICATION

Marc Baldus, Eelco T. C. Vogt *et al.*

A DNP-supported solid-state NMR study of carbon species in fluid catalytic cracking catalysts

ChemComm

COMMUNICATION

View Article Online
View Journal | View Issue

Cite this: *Chem. Commun.*, 2017, 53, 3933

Received 1st February 2017,
Accepted 3rd March 2017

DOI: 10.1039/c7cc00849j

rsc.li/chemcomm

A DNP-supported solid-state NMR study of carbon species in fluid catalytic cracking catalysts†

Deni Mance,[a] Johan van der Zwan,[a] Marjolein E. Z. Velthoen,[b] Florian Meirer,[b] Bert M. Weckhuysen,[b] Marc Baldus*[a] and Eelco T. C. Vogt*[bc]

A combination of solid-state NMR techniques supported by EPR and SEM-EDX experiments was used to localize different carbon species (coke) in commercial fluid catalytic cracking catalysts. Aliphatic coke species formed during the catalytic process and aromatic coke species deposited directly from the feedstock respond differently to dynamic nuclear polarization signal enhancement in integral and crushed FCC particles, indicating that aromatic species are mostly concentrated on the outside of the catalyst particles, whereas aliphatic species are also located on the inside of the FCC particles. The comparison of solid-state NMR data with and without the DNP radical at low and ambient temperature suggests the proximity between aromatic carbon deposits and metals (mostly iron) on the catalyst surface. These findings potentially indicate that coke and iron deposit together, or that iron has a role in the formation of aromatic coke.

Fluid catalytic cracking (FCC) is the main conversion technology used in oil refineries, converting heavy Vacuum Gas Oil (VGO) and residual feedstock to valuable transportation fuels like gasoline, and petrochemical raw materials like propylene. Approximately 14.5 million barrels of feedstock are converted in this process every day.[1] During commercial operation, FCC catalysts deactivate rapidly because of the deposition of carbon species. The harsh process conditions, with temperatures cycling between 720 °C in oxidative environment in the regenerator and 520–550 °C in the reducing environment in the riser reactor, enhance the deactivation. Typical contact times in the riser reactor are in the order of seconds, after which the catalyst has to be regenerated to remove the coke species that block the surface and pore system. Deposition of metals like iron, nickel, and vanadium during consecutive cycles may create (de-)hydrogenation activity, which further promotes coke formation.[2] Carbon deposition is not only a negative issue: regeneration of the catalyst by burning off the coke fuels the endothermic cracking reaction and the heat requirement for the process. The trick is thus to limit the amount of coke formed to the absolute minimum required for the thermal equilibrium of the process, also in order to limit the amount of CO_2 formed. However, in a quest to utilize as much of our fossil fuels as possible, heavier feedstocks, like vacuum residues, are more frequently employed. These heavier feedstocks contain more coke precursors, and will deposit more coke from the feedstock directly.[3]

Carbon deposition in catalytic processes has been studied extensively[4,5] using bulk techniques like TPO/TGA,[6] ^{13}C NMR,[7–12] (FT-)IR,[4,5] UV-Vis and confocal fluorescence microscopy,[13,14] NEXAFS,[15–17] EELS,[18] EPR,[5] PET,[19,20] XPS,[8] supercritical fluid extraction,[8] and MALDI-TOF-MS.[7,21]

Various authors have studied the development of coke species over time.[22–26] Cerqueira *et al.*[27] describe mainly two types of coke in FCC catalysts, *i.e.* coke directly deposited from the feedstock, and coke formed on the catalyst surface as a (secondary) result of the cracking process. These different types include hydrocarbons adsorbed on the catalyst surface and within the catalyst pores. It is very important to be able to distinguish between these two types. Carbon deposition from the feedstock can hardly be avoided, but with catalyst design we can control (*i.e.* limit) the coke that is formed during catalysis. Cerqueira *et al.*, in another paper,[28] describe the analysis of carbon deposited on FCC catalysts during cracking of residual feedstock using a variety of techniques, including ^{13}C MAS (Magic Angle Spinning) NMR.[29] They observe spectra consisting of a large contribution in the aromatic coke range (around 130 ppm) and a smaller signal around 18–20 ppm which is typical for aliphatic carbons.[12] They found that 80–90% of the carbon is in aromatic rings, and the remainder is in aliphatic groups. Based on the low H/C ratio observed, they conclude the aromatic structures must be relatively large. Similar observations were reported by Barth *et al.*[7] and Qian *et al.*[8] The work of

[a] *NMR Spectroscopy, Bijvoet Center for Biomolecular Research, Utrecht University, Padualaan 8, 3584 CH Utrecht, The Netherlands. E-mail: m.baldus@uu.nl*
[b] *Inorganic Chemistry and Catalysis, Debye Institute for Nanomaterials Science, Utrecht University, Universiteitsweg 99, 3584 CG Utrecht, The Netherlands. E-mail: e.t.c.vogt@uu.nl*
[c] *Albemarle Catalysts Company BV, Research Center Amsterdam, PO box 37650, 1030 BE Amsterdam, The Netherlands*

† Electronic supplementary information (ESI) available: Details of SEM-EDX analysis and EPR work and additional details of NMR-analysis. See DOI: 10.1039/c7cc00849j

Fonseca *et al.* on hydroprocessing catalysts[9] suggests young catalytic coke formed as a result of the cracking process is more aliphatic (older catalytic coke will likely be more aromatic). Snape *et al.*[12] suggest that coke deposited from heavy feedstocks is more aromatic. However, no direct data are currently available on the spatial distribution of the coke species within integral FCC catalyst particles.

Here we demonstrate the use of a dedicated solid-state NMR approach that involves the application of one- and two-dimensional MAS solid-state NMR experiments conducted at different temperatures in combination with Dynamic-Nuclear-Polarization (DNP)-supported solid-state NMR[30,31] to examine the spatial distribution of coke species in a commercial equilibrium FCC catalyst containing 1.75 wt% of coke, 0.65 wt% Fe, 950 ppm Ni, and 70 ppm V. The catalyst was selected from a database of equilibrium FCC catalysts based on its high carbon content. Catalyst particles were sieved to obtain a sieve fraction of 38–76 μm. Crushed catalyst material was obtained by crushing the FCC particles in a mortar. Previous work[32,33] has shown that additional line broadening under low-temperature DNP conditions only occurs due to freezing out of local molecular mobility and paramagnetic relaxation very close to that of the DNP radical itself. In the current situation, both effects can be neglected and we hence expect, similar to previous work,[34,35] spectroscopic resolution similar to conventional solid-state NMR experiments. While DNP-NMR has been performed before on solids and catalysts,[36–38] this paper is a first demonstration of the elusive speciation of coke in FCC catalysts using the technique.

In Fig. 1A, we compare DNP results obtained at 400 MHz for whole (Fig. 1A, top lines) and crushed (Fig. 1A, middle lines) FCC samples in reference to the free solvent. From the experimentally detected ^{13}C chemical shifts as well as from ^{1}H chemical shifts derived from an (^{1}H,^{13}C) FLSG-HETCOR[39] spectrum obtained under DNP conditions (Fig. 1B), we concluded, in line with earlier work,[7,8,28] that our ^{13}C spectra are dominated by aliphatic and aromatic ^{13}C moieties. Note that ^{13}C signals at about 150 ppm are missing in the HETCOR experiment that was recorded using a short Cross Polarization (CP) contact time, in line with the absence of quaternary carbons. As presented in Fig. 1A, we observed relative DNP signal enhancements varying between 2.5 and 4.6, with higher enhancements generally observed for crushed FCC particles.

While the relative signal enhancement for aromatic resonances only changed by about 13% between both preparations, we observed a significant increase of about 43% for the aliphatic peaks around 40 ppm. Assuming that the DNP enhancement is largely confined to the surface of our preparations (due to the low proton density),[35,40,41] these results suggest that a significant portion of aliphatic carbon must be embedded within the FCC particle and only becomes DNP active, *i.e.*, solvent exposed, after crushing. Barth *et al.*[7] and Qian *et al.*[8] assume that the aliphatic carbon and aromatic carbon are always constituent of the same molecules. Our results indicate that this is not necessarily the case.

Next, we examined whole FCC particles under 800 MHz/527 GHz DNP conditions and compared the results obtained to the 400 MHz DNP case. This is shown in Fig. 2. Including MAS

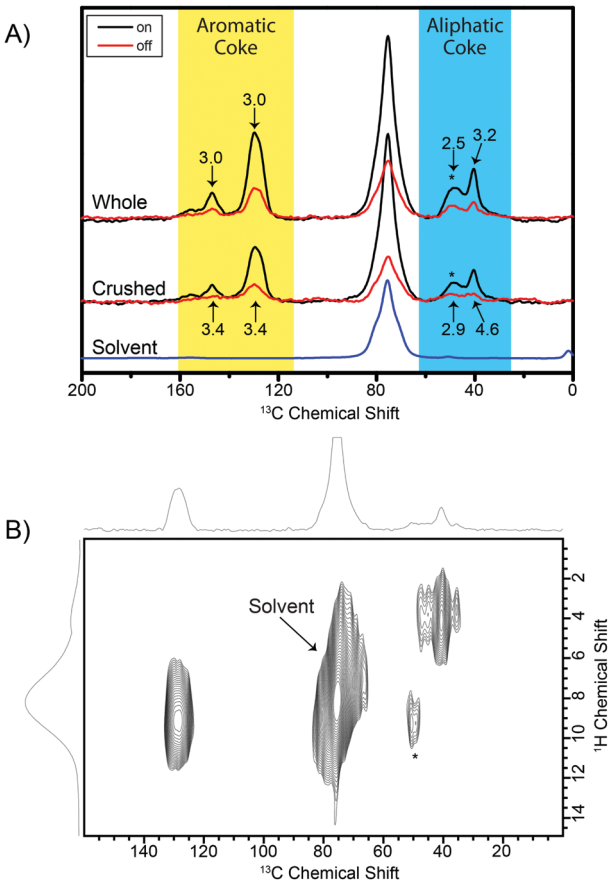

Fig. 1 (A) ^{13}C CP-MAS spectra measured on a 400 MHz DNP system at 100 K. Black represents spectra with irradiation of microwaves and red represents spectra without irradiation of microwaves. The top spectra are recorded on whole FCC particles, the middle spectra are recorded on crushed FCC particles. The blue spectrum was recorded on just the solvent used for wetting the sample. The numbers indicated represent the DNP-enhancements computed from the intensity ratios of on- and off-DNP experiments: the enhancement is strongest for the aliphatic signal in the crushed particles; (B) FLSG-HETCOR spectrum[39] of whole FCC particles under DNP condition using a short CP contact time of 50 μs.

sideband intensities at higher B_0 field, the relative NMR signal intensity between the aromatic and aliphatic signals remained largely constant. As expected,[42] DNP enhancements were reduced at 800 MHz compared to the data obtained at 400 MHz. In line with earlier results, the observed reduction was lower than that observed for AMUpol[43] which may be due to the smaller molecular size of Pypol leading to an, on average, stronger hyperfine coupling that determines the DNP transfer efficiency.[42]

Finally, we examined the influence of the biradical itself on our solid-state NMR spectra for two different temperatures. The results are shown in Fig. 3. In the absence of biradicals, the spectrum is dominated by aromatic signals both at high and lower temperatures and the relative increase in signal intensity is in line with thermodynamic predictions. Upon addition of Pypol, signal intensities strongly increase at lower temperatures (factor 40 in Fig. 3) and aliphatic contributions appeared that remained largely invisible in the absence of the biradical.

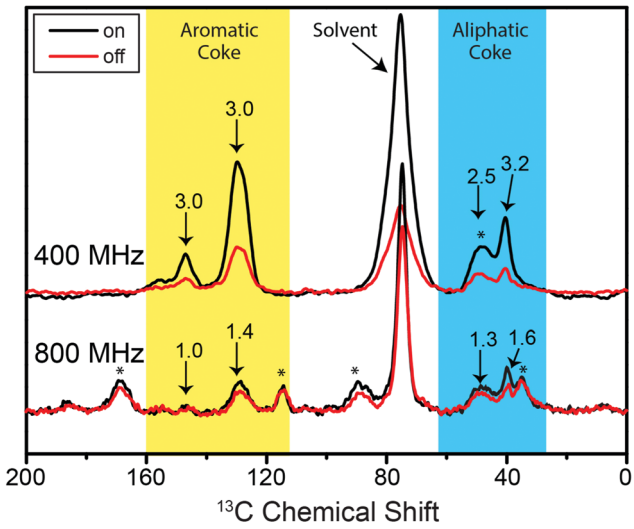

Fig. 2 ^{13}C CP-MAS spectra measured with the 400 MHz (top spectra) and 800 MHz (bottom spectra) DNP system at 100 K. Black lines represent the spectra with irradiation of microwaves, red lines represent spectra without irradiation of microwaves. MAS sidebands are indicated by *.

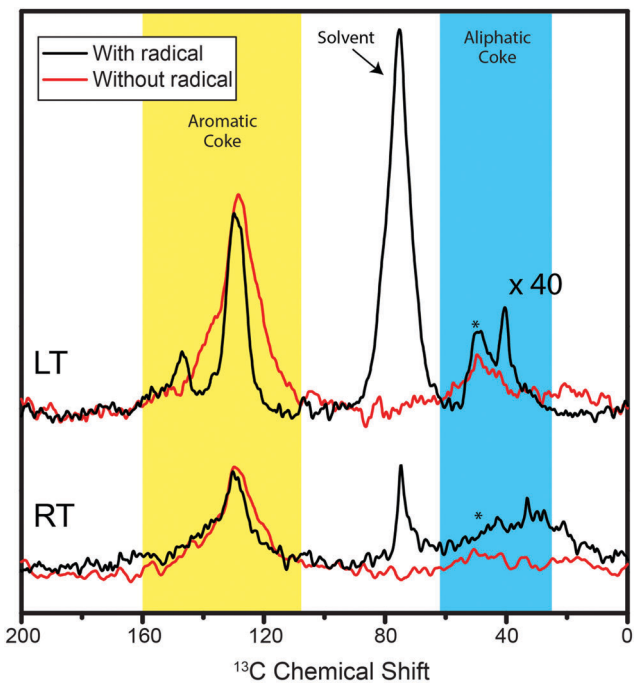

Fig. 3 ^{13}C CP-MAS spectra of FCC particles measured with the 400 MHz DNP system without microwaves. Black lines represent the spectra of the sample with the added radical and red lines represent spectra measured without the radical. The top lines (LT) represent the spectra measured at 100 K, the bottom lines (RT) depict the spectra measured at 293 K.

These results obtained in the absence of radical can be explained by (a) a dominant aromatic coke contribution compared to aliphatic species or (b) favourable relaxation properties for aromatic species possibly due to paramagnetic effects resulting from the proximity of *e.g.* metal(ion) species, such as Fe, V or Ni species. Upon addition of biradicals, surface species become dominant and they both contain aromatic and aliphatic ^{13}C moieties.

Previous work using (Scanning) Transmission X-ray Microscopy ((S)TXM), X-ray Fluorescence (XRF) and SEM has yielded strong evidence for the concentration of Fe and Ni in an outer shell of FCC equilibrium catalyst particles.[44–51] In order to corroborate these findings, we have conducted SEM-EDX analysis of the FCC catalyst material used in the NMR-studies. We find an increased concentration of iron in the outer shell with some variations between individual particles (see Fig. 4 and Fig. S1–S8, ESI†). Since the sample is an equilibrium catalyst with an age-distribution, it is not unexpected that the intra-particle metal distribution and inter-particle concentrations vary between the FCC particles.

In addition, we have performed EPR experiments, which show that iron is the dominant paramagnetic species present in the FCC catalyst particles (see Fig. S10, ESI†). The EPR shows a minor contribution from Mn, which is confirmed by SEM-EDX (Fig. S9, ESI†). The DNP experiments indicate a concentration of aromatic coke on the outside of the FCC particles, while SEM-EDX and EPR indicate that paramagnetic iron species are also concentrated on the outside of the FCC particles. The combination of these two sets of observations suggests that the effect observed in Fig. 3 can be explained mainly by paramagnetic relaxation effects.

We have described a tailored solid-state NMR approach, supported by EPR and SEM-EDX, that provides insight into the molecular environment of ^{13}C coke species: aromatic groups are largely surface exposed and contain a significant fraction that most likely is located close to a paramagnetic species, such as Fe. Likewise, aliphatic coke species are located at the surface of the FCC particle but they can also be found in the interior of the FCC particle and are located more distant from paramagnetic species compared to aromatic species. These experimental observations support a model where large heteroaromatic carbon species are preferentially deposited on the outer surface of the catalyst, and catalytic coke, more aliphatic in nature, is formed inside the catalyst particle. This first evidence of spatial distribution of the two different coke species (deposited from feedstock and formed during catalysis) provides valuable insight into the deactivation mechanism of the largest commercial catalytic process, and will eventually allow the most efficient use of our scarce raw materials.

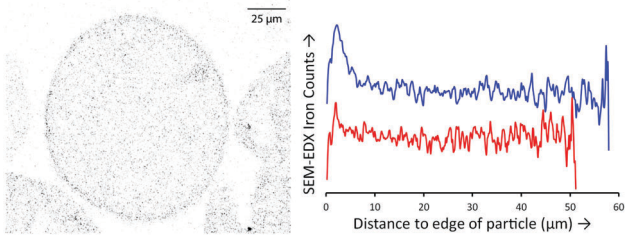

Fig. 4 SEM-EDX analysis of iron distribution in FCC particles. The left panel shows an iron greyscale-coded image. The relative concentration in the outer shell is obvious. The right image shows the radial distribution of iron as a function of distance to the edge of the particle (outer edge is to the left) for two different FCC particles.

Our studies also showcase the beneficial effect of using DNP in the context of *in situ* solid-state NMR material science studies providing the spectroscopic basis for further in-depth studies of FCC catalyst particles, for instance, by studying the effect of catalyst age on carbon deposition and formation, as well as more detailed localization and speciation of the carbon inside the catalyst particles as a function of catalyst age.

This research is part of the Strategic Theme Sustainability of Utrecht University and a related subsidy. The solid-state NMR/DNP studies were supported by the Netherlands Organization for Scientific Research (NWO) (grants 700.26.121 and 700.10.443 to M.B.). The authors thank Leo Woning for recording the SEM images. We are indebted to P. Tordo and his group for providing PyPol.

References

1 E. T. C. Vogt and B. M. Weckhuysen, *Chem. Soc. Rev.*, 2015, **44**, 7342–7370.
2 Y. Mathieu, A. Corma, M. Echard and M. Bories, *Appl. Catal., A*, 2014, **269**, 451–465.
3 A. Corma, L. Sauvanaud, E. Doskocil and G. Yaluris, *J. Catal.*, 2011, **279**, 183–195.
4 H. G. Karge, *Stud. Surf. Sci. Catal.*, 2001, **137**, 707–746.
5 M. Guisnet and P. Magnoux, *Appl. Catal.*, 1989, **54**, 1–27.
6 O. Bayraktar and E. L. Kugler, *Appl. Catal., A*, 2002, **233**, 197–213.
7 J.-O. Barth, A. Jentys and J. A. Lercher, *Ind. Eng. Chem. Res.*, 2004, **43**, 2368–2375.
8 K. Qian, D. C. Tomczak, E. F. Rakiewicz, R. H. Harding, G. Yaluris, W. C. Cheng, X. Zhao and A. W. Peters, *Energy Fuels*, 1997, **11**, 596–601.
9 A. Fonseca, P. Zeuthen and J. B. Nagy, *Fuel*, 1996, **75**, 1413–1423.
10 A. Fonseca, P. Zeuthen and J. B. Nagy, *Fuel*, 1996, **75**, 1363–1376.
11 A. Fonseca, P. Zeuthen and J. B. Nagy, *Fuel*, 1995, **74**, 1267–1276.
12 C. E. Snape, B. J. McGhee, J. M. Andresen, R. Hughes, C. L. Koon and C. Hutchings, *Appl. Catal.*, 1995, **129**, 125–132.
13 D. Mores, J. Kornatowksi, U. Olsbye and B. M. Weckhuysen, *Chem. – Eur. J.*, 2011, **17**, 2874–2884.
14 D. Mores, E. Stavitski, M. F. H. Kox, J. Kornatowski, U. Olsbye and B. M. Weckhuysen, *Chem. – Eur. J.*, 2008, **14**, 11320–11327.
15 H. Shimada, M. Imamura, N. Matsubayashi, T. Saito and T. Tanaka, *Top. Catal.*, 2000, **10**, 265–271.
16 M. A. Smith and R. F. Lobo, *Microporous Mesoporous Mater.*, 2006, **92**, 81–93.
17 S. M. Davis, Y. Zhou, M. A. Freeman, D. A. Fischer, G. M. Meitzner and J. L. Gland, *J. Catal.*, 1992, **139**, 322–325.
18 P. Gallezot, C. Leclercq, J. Barbier and P. Marecot, *J. Catal.*, 1989, **116**, 164–170.
19 N.-K. Bär, F. Bauer, D. M. Ruthven and B. J. Balcom, *J. Catal.*, 2002, **208**, 224–228.
20 B. G. Anderson, R. A. van Santen and L. J. van IJzendoorn, *Appl. Catal., A*, 1997, **160**, 125–138.
21 J. O. Barth, A. Jantys and J. A. Lercher, *Ind. Eng. Chem. Res.*, 2004, **43**, 3097–3104.
22 M. Den Hollander, M. Makkee and J. Moulijn, *Catal. Today*, 1998, **46**, 27–35.
23 M. Den Hollander, M. Makkee and J. Moulijn, *Stud. Surf. Sci. Catal.*, 1997, **111**, 295–302.
24 X. Dupain, M. Makkee and J. A. Moulijn, *Appl. Catal., A*, 2006, **297**, 198–219.
25 J. P. Hofmann, D. Mores, L. R. Aramburo, S. Teketel, M. Rohnke, J. Janek, U. Olsbye and B. M. Weckhuysen, *Chem. – Eur. J.*, 2013, **19**, 8533–8542.
26 M. A. Callejas, M. T. Martínez, T. Blasco and E. Sastre, *Appl. Catal., A*, 2001, **218**, 181–188.
27 H. S. Cerqueira, G. Caeiro, L. Costa and F. Ramôa Ribeiro, *J. Mol. Catal. A: Chem.*, 2008, **292**, 1–13.
28 H. S. Cerqueira, C. Sievers, G. Joly, P. Magnoux and J. A. Lercher, *Ind. Eng. Chem. Res.*, 2005, **44**, 2069–2077.
29 E. R. Andrew, A. Bradbury and R. G. Eades, *Nature*, 1958, **182**, 1659.
30 A. W. Overhauser, *Phys. Rev.*, 1953, **92**, 411–415.
31 Q. Z. Ni, E. Daviso, T. V. Can, J. Herzfeld and R. C. Griffin, *Acc. Chem. Res.*, 2013, **46**, 1933–1941.
32 E. J. Koers, E. A. W. van der Cruyssen, M. Rosay, M. Weingarth and A. Prokofyev, *et al.*, *J. Biomol. NMR*, 2014, **60**, 157–168.
33 E. A. W. van der Cruijsen, E. J. Koers, C. Sauvee, R. E. Hulse, M. Weingarth and O. Ouari, *et al.*, *Chem. – Eur. J.*, 2015, **21**, 12971–12977.
34 E. J. Koers, M. P. López-Deber, M. Weingarth, D. Nand, D. T. Hickman and D. Mlaki Ndao, *et al.*, *Angew. Chem., Int. Ed.*, 2013, **52**, 10905–10908.
35 A. Jantschke, E. Koers, D. Mance, M. Weingarth, E. Brunner and M. Baldus, *Angew. Chem., Int. Ed.*, 2015, **54**, 15069–15073.
36 W.-C. Liao, T. C. Ong, D. Gajan, C. Reiter, F. Engelke, D. L. Silverio, C. Copéret, M. Lelli, A. Lesage and L. Emsley, *Chem. Sci.*, 2017, **8**, 416–422.
37 S. R. Chaudhary, P. Berruyer, D. Gajan, C. Reiter and F. Engelke, *et al.*, *Phys. Chem. Chem. Phys.*, 2016, **18**, 10616–10622.
38 F. A. Perras, T. Kobayashi and M. Pruski, *J. Am. Chem. Soc.*, 2015, **137**, 8336–8339.
39 B.-J. Van Rossum, H. Förster and H. J. M. de Groot, *Magn. Reson.*, 1997, **124**, 516–519.
40 P. C. A. van der Wel, K.-N. Hu, J. Lewandowski and R. G. Griffin, *J. Am. Chem. Soc.*, 2006, **128**, 10840–10846.
41 A. J. Rossini, A. Zagdoun, M. Lelli, A. Lesage, C. Copéret and L. Emsley, *Acc. Chem. Res.*, 2013, **46**, 1942–1951.
42 D. Mance, P. Gast, M. Huber, M. Baldus and K. L. Ivanov, *J. Chem. Phys.*, 2015, **142**, 234201.
43 C. Sauvee, M. Rosay, G. Casano, F. Aussenac, R. T. Weber, O. Ouari and P. Tordo, *Angew. Chem., Int. Ed.*, 2013, **52**, 10858–10861.
44 F. Meirer, S. Kalirai, D. Morris, S. Soparawalla, Y. Liu, G. Mesu, J. C. Andrews and B. M. Weckhuysen, *Sci. Adv.*, 2015, **1**, e1400199.
45 Y. Liu, F. Meirer, C. M. Krest, S. Webb and B. M. Weckhuysen, *Nat. Commun.*, 2016, **7**, 12634.
46 F. Meirer, S. Kalirai, J. N. Weker, Y. Liu, J. C. Andrews and B. M. Weckhuysen, *Chem. Commun.*, 2015, **51**, 8097–8100.
47 F. Meirer, D. T. Morris, S. Kalirai, Y. Liu, J. C. Andrews and B. M. Weckhuysen, *J. Am. Chem. Soc.*, 2015, **137**, 102–105.
48 S. Kalirai, U. Boesenberg, G. Falkenberg, F. Meirer and B. M. Weckhuysen, *ChemCatChem*, 2015, 3674–3682.
49 A. Wise, J. N. Weker, S. Kalirai, M. Farmand, D. A. Shapiro, F. Meirer and B. M. Weckhuysen, *ACS Catal.*, 2016, **6**, 2178–2181.
50 S. Kalirai, P. P. Paalanan, J. Wang, F. Meirer and B. M. Weckhuysen, *Angew. Chem., Int. Ed.*, 2016, **55**, 11134–11138.
51 E. Rautiainen and B. Nelissen, *Hydrocarbon Eng.*, April 2013, 41–47.

